ELSEVIER

Physica C 331 (2000) 57–66

PHYSICA C

www.elsevier.nl/locate/physc

Hysteresis of the critical current density in YBCO, HBCCO and BSCCO superconducting polycrystals: a comparative study

A.J. Batista-Leyva [a,b,*], R. Cobas [a], E. Estévez-Rams [c], M.T.D. Orlando [d], C. Noda [a], E. Altshuler [a]

[a] *Superconductivity Laboratory, IMRE-Physics Faculty, University of Havana, 10400 Havana, Cuba*
[b] *Physics Department, Engineering Faculty, University of Holguín, 80100 Holguín, Cuba*
[c] *Laboratory for Structural Analysis, IMRE-Physics Faculty, University of Havana, 10400 Havana, Cuba*
[d] *Physics Department, Universidade Federal do Espiritu Santo, Vitoria-ES 29060-900, Brazil*

Received 20 May 1999; received in revised form 14 June 1999; accepted 22 September 1999

Abstract

The hysteresis of the transport critical current of $YBa_2Cu_3O_{7-\delta}$ (Hg,Re)$Ba_2Ca_2Cu_2O_{8+\delta}$ and $(BiPb)_2Sr_2Ca_2Cu_3O_{10+\delta}$ polycrystals was studied. While the first two systems display qualitatively similar hysteretical patterns, the third one behaves differently. The experimental results are interpreted in terms of a phenomenological model which considers the effects of the magnetization in the grains on the intergranular weak links as responsible for the observed hysteresis.

The hysteresis of the transport critical current is discussed on the light of the microstructural features of the samples, concluding that the shape and disposition of the grains do not account in a straightforward fashion for the differences in the hysteretical behavior.

Keywords: Hysteresis; YBCO; HBCCO; BSCCO

1. Introduction

The study of the dependence of transport properties with an applied magnetic field in ceramic superconductors has proven to be a powerful tool in the understanding of a variety of characteristics of High Temperature Superconductors (HTc).

An important fraction of these studies has been devoted to the hysteretical behavior of $J_c(B_a)$ in polycrystalline HTc's at low fields, for instance $YBa_2Cu_3O_{7-\delta}$ (YBCO) [1] and $(BiPb)_2Sr_2Ca_2Cu_3O_{10+\delta}$ (Bi-2223) [2,3]. The model of Peterson and Ekin [4], developed qualitatively by Evetts and Glowacki [5], stated the theoretical basis for the explanation of these phenomena. This model, put on more quantitative roots by Altshuler et al. [1] and by Müller and Mathews [6], has been applied in the understanding of the hysteretical behavior of J_c in ceramic superconductors. Following that model, the hysteresis may be explained in terms of the effect of the flux trapped by the superconducting grains on the intergrain weak links, which produces different values of the average effective field at the junctions for

* Corresponding author. Superconductivity Laboratory, IMRE-Physics Faculty, University of Havana, 10400 Havana, Cuba.
E-mail addresses: supercon@imre.oc.uh.cu (A.J. Batista-Leyva), abatista@uho.hlg.edu.cu (A.J. Batista-Leyva).

0921-4534/00/$ - see front matter
PII: S0921-4534(99)00589-4

increasing and decreasing applied fields. This irreversibility of the effective field at the junctions is a fingerprint of the hysteresis of the intragranular magnetization. No report of the hysteresis of $J_c(H)$ has been published for $HgBa_2Ca_2Cu_2O_{8+\delta}$ and related ceramics (Hg-1223), as far as we know.

In the present paper, a comparative study of the hysteretical behavior of YBCO, Hg-1223 and Bi-2223 ceramics is carried out. The results for the different systems are compared and quantitatively explained in terms of flux trapping by the superconducting grains. This approach has been successfully applied to the explanation of relaxational effects in YBCO and Hg-1223 polycrystals [7]. An attempt is made to understand the differences in the hysteretical behavior of the superconducting ceramics based on the particularities in their microstructure.

2. Experimental

2.1. Sample preparation and properties

All the samples were prepared by the conventional ceramic route. The details for each system are as follows.

YBaCuO: High quality powders of Y_2O_3, $BaCO_3$ and CuO were mixed in stoichiometric proportions, the ratio of Y:Ba:Cu in the original powders being 1:2:3. These raw materials were calcinated during 16 h at 900°C, 920°C and 940°C. At the end of each step, the powders were grounded in a mill. After that, they were pressed into pellets at 300 MPa, sintered at 950°C for 24 h, and cooled down to room temperature at a rate of 1°C/min in air. Bars of approximately $10 \times 1 \times 1$ mm^3 were cut from the pellets.

The onset critical temperature, defined as the maximum in the $d\rho/dT$ curve is $T_{c0} = 90.1$ K, and the zero resistance critical temperature without external magnetic field is $T_z = 86.8$ K. As can be seen, both values are depressed in comparison with the ones usually reported in literature, so the absence of oxygenation during the cooling process affects both intragranular and intergranular properties. Anyway, the most affected is T_z (closely related with the intergranular ones [8]), taking into account that the grain boundary is the zone with stronger stoichiometric affectations, even in oxygenated samples. The critical current density at zero applied field was 65 A/cm^2.

Hg-1223: $BaCO_3$, $CaCO_3$, CuO and ReO_2 high purity powders were prepared in a 2:2:3:0.18 stoichiometric mixture. The mixture was first homogenized in an agate mortar and thermally treated at 850°C for 12 h under oxygen flux. After this, the material was crushed in an agate mortar and pelletized under 1 GPa. The pellets were submitted to calcination at 930°C for 15 h under oxygen flow. The latter procedure was repeated crushing the mixture between calcination treatments. The precursors were then treated at 930°C for 12 h using 20% oxygen and 80% argon flow. High purity HgO was added to the final mixture and homogenized in an agate mortar. The powder was pelletized uniaxially under 1 GPa, using a vacuum pump to reduce the gas present inside the pellet. It was immediately introduced inside a gold foil and both inside a quartz tube of 0.8 cm in inner diameter, with a filling factor of 1.1 g/cm^3 [9]. The tube was sealed under vacuum (10^{-2} Torr), and introduced inside an isostatic pressure furnace with 40 bar of argon. The sample was heated at a rate of 300°C/h until 700°C, at 120°C/h until 850°C and hold at this temperature for 15 h. Then the furnace was cooled down at 120°C/h to 30°C. Bars of approximately $10 \times 1 \times 1$ mm^3 were cut from the pellets.

The values of critical temperatures are $T_{c0} = 133.6$ K and $T_z = 129.1$ K. Those values are close to the usually reported ones for the Hg based undoped ceramics [10], meaning that the addition of Re did not affect the critical temperature of the superconductor. The obtained value of T_{c0} is close to that of Reder et al. [11] for Hg-1223 ceramics, with Re content not far from ours. The critical current density with no applied magnetic field was 34.7 A/cm^2, far from the best values of these ceramics.

Bi-2223: High purity powders of the starting materials Bi_2O_3, PbO_2, $SrCaO_3$, $CaCO_3$ and CuO were mixed in a stoichiometric ratio Bi:Pb:Sr:Ca:Cu of 1.6:0.4:2:2:3. The powders were thermally treated at 700°C, 750°C and 800°C. At the end of each treatment, the pellets were manually grounded. The powders were pressed into pellets at 400 MPa and the sintering was carried out at a temperature of 848°C for 48 h; the samples were then cooled down to

room temperature at a rate of 1°C/min · in air. Bars of approximately $10 \times 1 \times 1$ mm^3 were cut from the as sintered pellets.

The values of critical temperature was $T_{c0} = 102.1$ K, and $T_z = 96.0$ K (without external field). Both values are considerably lower than those reported by Muné et al. [2,12] in ceramics sintered by similar route. This can be related to two different facts: first, the impossibility of controlling the oxygen content in the ceramic, which, according to Emmen [13] can reduce T_{c0} even to 80% of its nominal value. Second, there are indications in the semi-qualitative analysis performed with back scattered electrons that Sr have been segregated from the grain to the intergranular region, which can be also partially responsible for the decrease in critical temperatures. The critical current density without external field was 8 A/cm^2, also well below the potentialities of these ceramics. The differences between our ceramics and those of Muné et al. [2,12] are important and will be discussed below.

2.2. Measurements

The J_c measurements were performed by the four-probe technique, with an automatic control of the sample temperature, the applied magnetic field and the bias current. The measurement of the sample's voltage was also controlled by a microcomputer. The temperature in the sample is set by a temperature controller which warrants that the temperature oscillations in the sample are within ± 0.02 K, and ± 0.2 K in static and dynamic regimes, respectively. The magnetic field was generated by a long solenoid and the sample was located in such a way that the applied field was uniform and perpendicular to the bias current. The bias current is pulsed and bipolar, the ON/OFF relation being 0.13 ms/2.7 ms, which yields a frequency of 176.6 Hz, far enough from the cutoff frequency of the lock-in amplifier that measures the voltage. The communication between the computer, the temperature control and the lock-in amplifier is performed with an interface IEEE-488. The details of the setup are described elsewhere [14]. The programs that control the operations are all designed with the same philosophy: after the application of any magnetic field history to the sample, the critical current is measured by varying the current injected to the superconductor, in such a way that certain voltage criterion (1 μV) is dynamically met by means of a PI control loop. In this way, three different kind of measurements where carried out, as follows.

Flux trapping curve: After erasing the previous magnetic history, the sample was Zero Field Cooled (ZFC) to the measurement temperature, the desired maximum field value was set and after few seconds, the field was turned off. Then, the critical current density was measured.

Virgin curve: After erasing the previous magnetic history, the sample was ZFC to the measurement temperature, and the field was increased with a variable sweep rate: 1 Oe/min ($H_{app} < 5$ Oe); 5 Oe/min (5 Oe $< H_{app} <$ 20 Oe) and 20 Oe/min ($H_{app} > 20$ Oe). This was done in order to minimize the errors that may appear due to the delay of the PI in the first portion of the J_c vs. H_{app} curves, where the $J_c(H)$ rate of variation is high. The critical current was measured every second.

Returning curves: After erasing the previous magnetic history, the sample was ZFC, a maximum value (H_m) was set, and after a few seconds, the field was decreased with a variable sweep rate (the same as in the virgin curves) to zero. The critical current was measured every second. Two different kind of curves can be obtained: *unsaturated*, when the increase of the H_m causes variations in the shape of the curve, and *saturated*, when the increase of H_m does not affect the curve.

Microstructural studies were carried out using a Jeol JSM-T 330A scanning electron microscope fitted with an energy dispersive microanalysis system. Backscattered electron signal was used.

3. Phenomenological theory

A widely employed model for the interpretation of the $J_c(H)$ characteristics in high T_c superconducting ceramics was proposed firstly by Peterson and Ekin in 1988 [4], considering that the weak links in the material can be regarded as a parallel network of Josephson Junctions with a statistical distribution of junction widths. Altshuler et al. [1], and Müller and Mathews [6] introduced the possibility of calculating the $J_c(H)$ characteristic under any magnetic history.

Basically, the model considers that the transport properties of the junctions are determined by an ''effective field'', H_{eff}, resulting from the superposition of the external applied field and the field associated with the magnetization of the superconducting grains. The grains are supposed to follow Bean's critical state model, generalized to consider the existence of the grains first critical field. The critical current is a function of the applied field, the maximum applied field (when the field is diminishing or is set to zero after a field excursion), the temperature and the time (if flux creep effects are considered). This dependence can be written, according Müller and Mathews [6], as:

$$\frac{I_{\mathrm{c}}(H,H_{\mathrm{m}},T)}{I_{\mathrm{c}}(T)} = \int_{G_{\min}}^{G_{\max}} \left| \frac{\sin\left(\frac{\pi H_{\mathrm{eff}}(G,H,H_{\mathrm{m}},T)}{H_0(T)}\right)}{\left(\frac{\pi H_{\mathrm{eff}}(G,H,H_{\mathrm{m}},T)}{H_0(T)}\right)} \right| \Gamma(G)\,\mathrm{d}G \quad \text{if} \quad H_{\mathrm{eff}} \le \frac{H_0}{2}, \tag{1a}$$

$$\frac{I_{\mathrm{c}}(H,H_{\mathrm{m}},T)}{I_{\mathrm{c}}(T)} = \int_{G_{\min}}^{G_{\max}} \left| \frac{H_0(T)}{\pi H_{\mathrm{eff}}(G,H,H_{\mathrm{m}},T)} \right| \Gamma(G)\,\mathrm{d}G \quad \text{if} \quad H_{\mathrm{eff}} \ge \frac{H_0}{2}, \tag{1b}$$

where G is a geometrical factor that depends on the microstructure of the sample, with values between -1 and 1, distributed according to $\Gamma(G)$ [15], and H_0 is the effective field value at which the first minimum appears in the $I_{\mathrm{c}}(H)$ pattern of a single junction. $I_{\mathrm{c}}(T)$ is the temperature dependent transport critical current. The values of H_{eff} are described by different expressions, depending on the sample's magnetic history. In expressions (1a) and (1b) the time dependence is not explicitly written, due to the fact that is not interesting for the interpretation of our experiments.

Applying the mean value theorem, the normalized current can be calculated as:

$$\frac{I_{\mathrm{c}}(H,H_{\mathrm{m}},T)}{I_{\mathrm{c}}(T)} = \left| \frac{\sin\left(\frac{\pi H_{\mathrm{eff}}(G_{\mathrm{av}},H,H_{\mathrm{m}},T)}{H_0(T)}\right)}{\left(\frac{\pi H_{\mathrm{eff}}(G_{\mathrm{av}},H,H_{\mathrm{m}},T)}{H_0(T)}\right)} \right| \text{if} \quad H_{\mathrm{eff}} \le \frac{H_0}{2}, \tag{2a}$$

$$\frac{I_{\mathrm{c}}(H,H_{\mathrm{m}},T)}{I_{\mathrm{c}}(T)} = \left| \frac{H_0(T)}{\pi H_{\mathrm{eff}}(G_{\mathrm{av}},H,H_{\mathrm{m}},T)} \right| \text{if} \quad H_{\mathrm{eff}} \ge \frac{H_0}{2}, \tag{2b}$$

where G_{av} is a value that belongs to the G's distribution. These expressions simplify the calculation, and save time when high accuracy is not a determining factor. The formulas for H_{eff} are taken from Refs. [1] and [6]. The combination of expressions (1a), (1b) (or (2a), (2b)) with the proper expressions for H_{eff} according to the magnetic history gives the $I_{\mathrm{c}}(H)$ dependence, which can be compared with experimental results.

The fitting procedure was the following: a triangular $\Gamma(G)$ distribution was selected, taking into account that its mean value equals the value that yields the maximum of the saturated returning curve, for which the effective field [1,6] is:

$$H_{\mathrm{eff}} = \frac{H - \langle G \rangle \frac{H^*}{2}}{1 - \langle G \rangle}$$

and that the maximum is reached when $H_{\mathrm{eff}} = 0$. From the fit of the virgin curve to (1a) and (1b), a fine tuning of the parameters of the distribution was performed. This distribution is employed for the fit of the returning as well as the flux trapping curves. For the flux trapping curve, which involves several expressions of H_{eff}, the expressions (2a) and (2b) were employed.

4. Results and discussion

4.1. Microstructure

In Fig. 1 the SEM images of the three superconducting ceramics are displayed. The YBCO micrograph is shown in Fig. 1(a). Its main features are typical of this kind of ceramics. Two population of grains were identified, one with average size of 200 μm (not observed in the SEM picture), and a smaller one with a mean grain size of 7.5 μm, with good connectivity between grains and relatively dense packing.

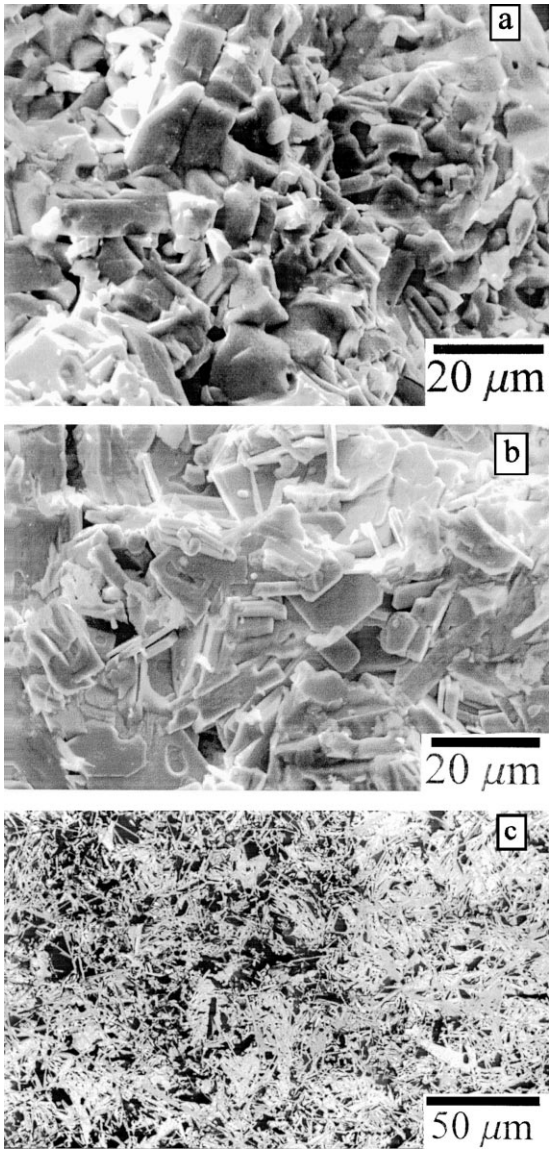

Fig. 1. (a) SEM micrograph of the YBCO sample. (b) SEM micrograph of the Hg-1223 sample. (c) SEM micrograph of the Bi-2223 sample.

Fig. 1(b) shows the micrograph of the Hg-1223 sample. There can be seen a region with plate like piled grains and another region with grains of thicker cross section, both with good connectivity between grains. The little spherical grains are inclusions of $CaHgO_2$ while the cylinder like are $Ba_2Cu_3O_5$ inclusions. The mean grain size is 10 μm.

Fig. 1(c) displays the micrograph of Bi-2223. A homogeneous, needle shaped grains population is present, with a mean size of 2.7 μm and low connectivity between grains. Also, the grain packing is of low density. These effects also contribute to the lowering of the critical temperature. Microanalysis shows the presence of a non-superconducting second phase composed of grains with rectangular cross section.

As can be seen, the microstructure of the samples under study are clearly different. It is interesting to note that the microstructure of Bi-2223 sample is completely different when compared with those reported by Muné et al. [2,12] which had plate-like, partially textured grains.

4.2. Transport measurement

4.2.1. YBCO

The flux trapping curve of YBCO at 80 K is shown in Fig. 2. Vertical arrows are pointing to the first critical field H_{c1g} (50 Oe) and the saturation field of the curve (350 Oe); so, the saturation field of the grains H^* (after Altshuler et al. [16]) is 150 Oe. The H_{c1g} obtained value is in good agreement with that reported by Altshuler [17] employing the flux trapping curve and Vibrating Sample Magnetometry, but H^* is bigger than his value. Calculating the intragranular critical current density with the help of Bean's model [18] yields 1.5×10^5 A/cm^2 in excellent agreement with Ref. [17], and of the same order of magnitude of other results in the same compound [16].

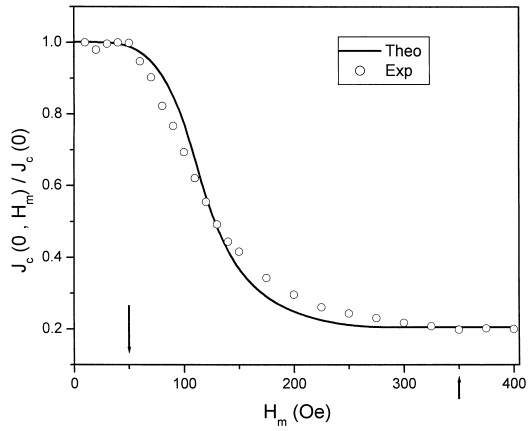

Fig. 2. Flux trapping curve for the YBCO sample. The line is a theoretical fit (see text).

The continuous line in Fig. 2 represents the fit done with the model. The agreement is good, and the main characteristics of the experimental curve are displayed by the theoretical one.

In Fig. 3 the virgin curve as well as several returns, for different values of H_m (ranging from $H_m < H_{c1g}$ to $H_m > H_{c1g} + 2H^*$) are displayed. As can be seen, the returning curve for $H_m < H_{c1g}$ almost exactly reproduces the virgin curve. The curves for $H_m > H_{c1g}$ show hysteretical effects whose magnitude grow with H_m. The main features of these curves agree with those obtained by Altshuler et al. for $J_c(H)$ in YBCO [1] and by Flores et al. [19] and Batista-Leyva et al. [20] for the hysteretical behavior of zero resistance critical temperature in YBCO, and are:

- The virgin curve has a maximum at $H_{app} \neq 0$ Oe and the returning ones at $H_{app} \neq 0$ Oe.
- With the increment of H_m, the maximum of the returning curves shift toward greater values of H_a, and the maximum value of $J_c(H)$ diminishes.
- When increasing H_m, a saturation value H_{ms} is found such that, for $H_m > H_{ms}$, there is no change in the shape of the returning curves.
- The average value of $|dJ_c/dH_a|$ is higher in the virgin curve than in the returning ones; the greater is the maximum field, the lower are the slopes in the returning curves.

Fig. 4 shows the least squares fit of virgin and saturated return curves to the theoretical model; a triangular distribution of geometrical factors with $G_{min} = -0.17$, $G_{max} = 0.9$ and $G_{peak} = 0.17$ (that yields the G_{av} taken for the fit of the flux trapping) was employed. This distribution is similar to that used in Ref. [17], and includes negative geometrical factors, related to the existence of zones with compression of intergrain magnetic flux [2]. As can be seen, the model reproduces quite well the main features of the experimental curves. The coincidence is remarkable, taking into account the fact that only slight variations in H_0 were needed when switching from the virgin to the flux trapping curves.

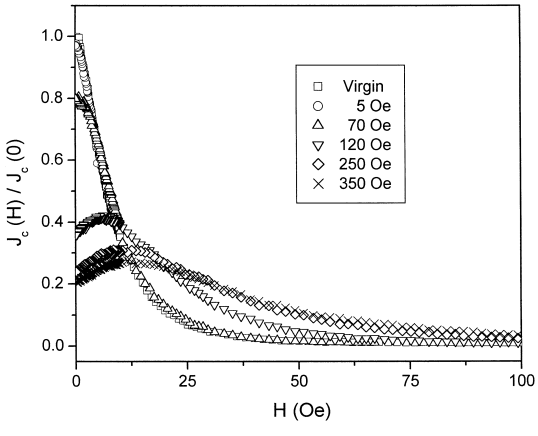

Fig. 3. Virgin and returning curves for the YBCO sample. The inset shows maximum field values for the returns.

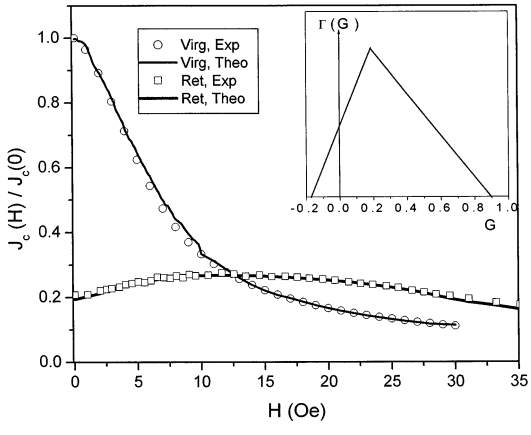

Fig. 4. Virgin and saturated return for YBCO. The lines are theoretical fits (see text). The inset shows the distribution of geometrical factors.

4.2.2. Hg-1223

In Fig. 5 the flux trapping curve for Hg-1223 is shown. The continuous line is the theoretical fit. There are several interesting features in the interpretation of this curve.

Firstly, it is remarkable the behavior for fields $H_a < 30$ Oe. The peak (shown in the inset of Fig. 5) that appears in this zone has never been reported in transport measurements, as far as we know, and can be interpreted in terms of intergranular flux trapping. In this sense it could be the ''decreasing tail'' of the intergranular flux trapping curve, and the saturation field would be (following this interpretation) $H_{sj} = 20$ Oe. Taking into account the fact that the first critical field of the intergranular region is expected to be very small ($H_{c1j} \approx 1$ Oe [21]), the intergranular critical current density must be of the order of 45 A/cm^2, in good agreement with the transport critical current determined by the experiment. Evidences of intergranular flux trapping had been found by Zhukov et al. [22] via magnetometric measurements. However, the authors could not measure the tail in transport measurements, due (according to them) to the intergranular flux loop breaking effect of the transport current. The fact that the intergranular activation energy for this ceramics is high (several eV for fields ≤ 5 Oe, as determined by ac susceptometry [23]) helps in the preservation of the intergranular flux trapping loops in the presence of transport currents. Needless to say, the fitting of our model does not take into account this tail. Then, only the intragranular part of the flux trapping curve is well fitted by the model.

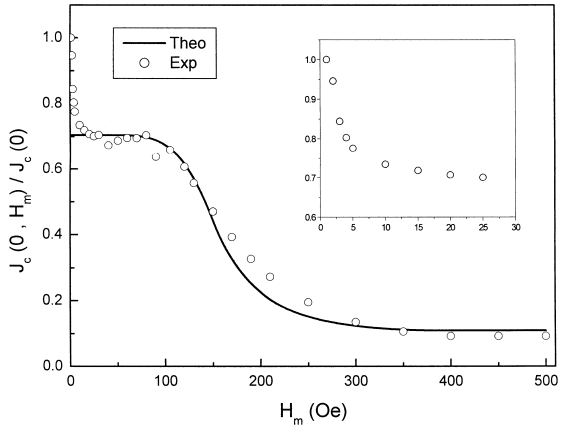

Fig. 5. Flux trapping curve for the Hg-1223 sample. The line is a theoretical fit (see text). The section corresponding to the first 30 Oe is plotted in the inset.

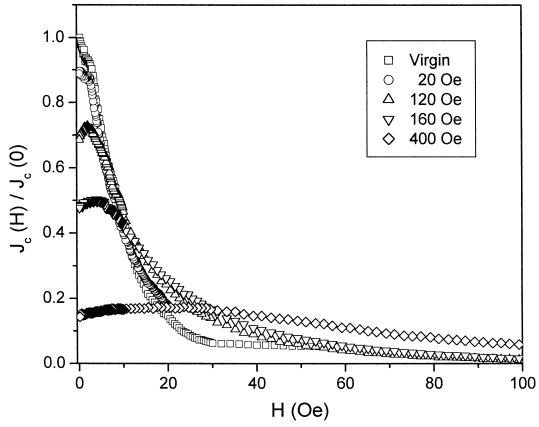

Fig. 6. Virgin and returning curves for the Hg-1223 sample. The inset shows the maximum field value for the returns.

Secondly, according to the usual interpretation of the flux trapping curve [16], $H_{c1g} \approx 100$ Oe and $H_s = 400$ Oe, so $H^* \approx 150$ Oe, the intragranular critical current density being 2.4×10^5 A/cm^2. However, we must be careful in the interpretation ofthe end of the first plateau, identified with H_{c1g}. In the Hg based superconducting polycrystals, the presence of surface barriers has been reported [24,25], whose action implies that the vortex will penetrate the grain at a field $H_p > H_{c1g}$:

$$H_p = H_c(T)\exp\left\{-\frac{T}{T_0}\right\},$$

where

$$H_c = \frac{\phi_0}{4\pi\lambda\xi}.$$

H_c is the thermodynamic critical field; λ and ξ are the London penetration depth and coherence length, respectively, and T_0 is a fitting constant [25]. Even for $H > H_p$, the surface barrier still impedes the entry and exit of vortices, resulting in a magnetization that slowly decays towards its equilibrium value [24]. It means that the first critical field has a lower value than the end of the first plateau in the flux trapping curve (100 Oe).

The above expressed facts mean that the interpretation of the flux trapping curves in the Hg based

superconducting ceramics needs to be reanalyzed. This will be done elsewhere.

In Fig. 6 the virgin as well as several return curves are plotted. It is interesting to note the kinks of the virgin and the first return curves ($H_m = 20$ Oe) for low fields. This can be also related to the intergranular flux trapping. However, even when the flux trapping curves for the Hg-1223 system have the above mentioned particularities, the qualitative description of the different kinds of returning curve is related to the flux trapping curve in the same way the rest of the systems do, the field at which the grain is penetrated being important.

The curves in Fig. 6 fulfill the same characteristics of those for YBCO (see Fig. 2), i.e., they show a strong hysteretical behavior.

In Fig. 7 the fit of the virgin and the saturated return curves is displayed. The distribution of geometrical factors (shown in the inset of the figure) is similar to that used for YBCO, except for the peak value, $G_{peak} = 0.26$. This choice is related to the fact that the maximum in the saturated returning curve is reached for a higher value of H than for YBCO. The fit is also very good in this case.

All the measurements performed in this compound, as well as the fitting to our model, are reported for the first time to our knowledge.

4.2.3. Bi-2223

Fig. 8 represents the flux trapping curve of Bi-2223. The main characteristic is the low value of the first critical field (6 Oe), the saturation field being 120 Oe. It yields $H^* = 57$ Oe, corresponding to an intragranular critical current density of 1.7×10^5 A/cm^2. In Ref. [2], the value obtained was 3.74×10^5 A/cm^2, reaffirming the idea that the intragranular properties of the ceramic are affected. It should be noted that it was *impossible* to fit that curve with the $\langle G \rangle$ value obtained from the saturated returning curve. Even taking $\langle G \rangle$ as a fitting parameter, the fit is quite unsatisfactory. This is coincident with the report of Muné and López [26], which needed to include in the model a series parallel network of Josephson Junctions to obtain a good fit of the flux trapping curves in Bi-2223.

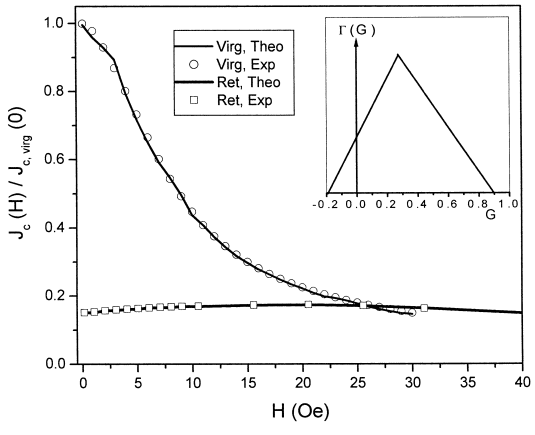

Fig. 7. Virgin and saturated return for the Hg1223 sample. The lines are theoretical fits (see text). The inset shows the distribution of geometrical factors.

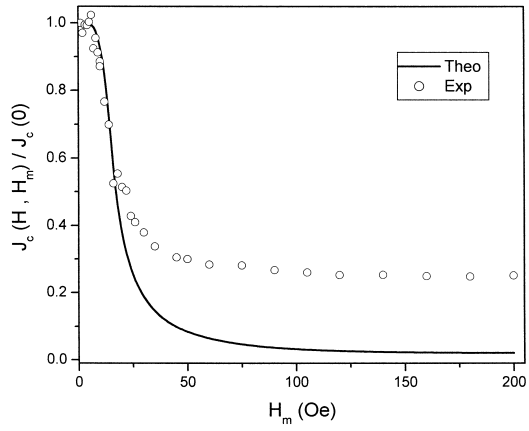

Fig. 8. Flux trapping curve for Bi2223. The line is a fit to the model (see text).

In Fig. 9 the virgin and some returning curves are shown. The most remarkable features of these curves are:

- The maxima of the virgin and the return curves are located at $H_a = 0$ (thus implying $\langle G \rangle \approx 0$).
- For fields higher than 8 Oe, the curves are very close one to each other, the hysteresis being considerably weaker than in YBCO and Hg-1223.
- Though the flux trapping curve yields $H_{c1g} \approx 6$ Oe, the returning curve for $H_m = 5$ Oe departs considerably from the virgin one.

The first two points are in complete agreement with other reports for this system [2,3,12,26]. The last point deserves further attention. The reason for this contradiction may be related to the character-

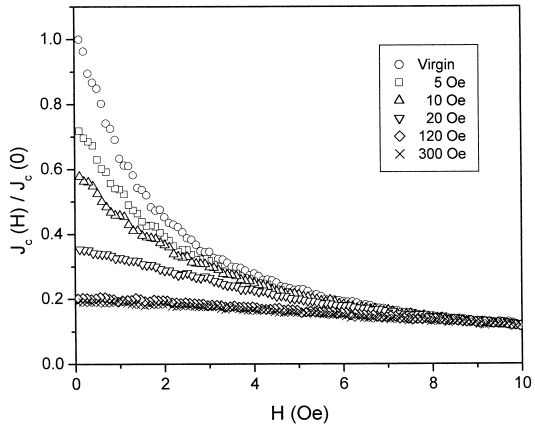

Fig. 9. Virgin and returning curves for the Bi-2223 sample. The inset shows the maximum field value for the returns.

istics of the sample and the measurement ''history''. As was stated before, the sintered Bi-2223 samples have low connectivity between grains and both the critical current density ($H_{app} = 0$) and zero resistance critical temperature are low, reflecting the poor properties of the intergranular region. It is possible that the transport properties of this region have been deteriorated during the measurement process, that was carried out in the following order: first, the virgin curve; second, the flux trapping and, at the end, the returning curves. So the latter ones were the most affected.

The differences in hysteresis between Bi-2223 and both YBCO and Hg-1223 are striking. The differences between YBCO and Bi-2223 (and the differences in the corresponding distributions of geometrical factors) have been pointed out by Muné et al. [2,12], arguing that they could be related to the differences in the microstructure of the samples. In the case of Bi-2223, the tendency of plate like growth in grains, as well as the texturing in their disposition (c axis alignment in the direction of compression during the fabrication process) gives rise to the existence of zones of compressed as well as decompressed magnetic flux, resulting in the weak hysteresis [2,26,27]. However, in the present case the situation is different. The Bi-2223 grains are so weakly and randomly connected that it is difficult to think in terms of flux compression or decompression in the style of the ''brick wall model'' [2,12]. However, the hysteretical behavior is the same than that of other works [2,27] in which ''good ceramics'' were employed. At the same time, the Hg based ceramics also have plate like grains, with a tendency of growing face to face, and the ceramic we employed is partially textured, as can be concluded from the inspection of Fig. 1(b) and other micrographs not presented here. Nevertheless, the Hg-1223 shows a hysteretical behavior (and a G distribution) that resembles that of YBCO, with a completely different grain morphology. Similar results were found in Ref. [20] for the hysteresis of the zero resistance critical temperature in the same kind of ceramics. The electron microscopy of those samples also shows differences in microstructure between them that cannot be correlated with the behavior of the transport critical current density in the presence of external magnetic field. This is coincident with an early report of Atlshuler et al. [28], where they found that for YBCO samples with identical microstructure (as shown in microphotographs), the shape of $J_c(H)$ curves was different, concluding that the superconducting properties of grains and junctions must be of more importance in the interpretation of their results, than the pure geometrical factors.

In Fig. 10 the fits of the virgin and the returning curves are displayed. It is easy to note that the fit is not quite good, specially in the returning curve, for which it was impossible to improve the fit shown if

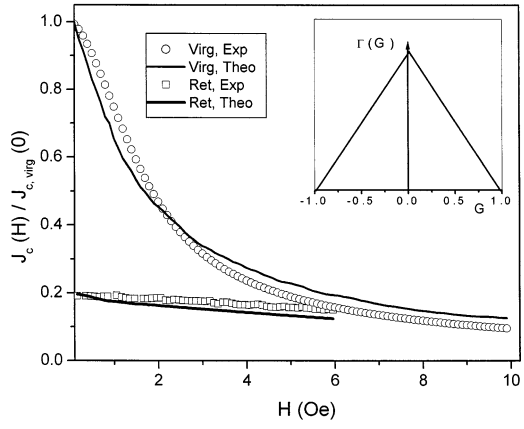

Fig. 10. Virgin and saturated return for the Bi-2223 sample. The lines are theoretical fits (see text). The inset shows the distribution of geometrical factors.

the condition of coincidence of the theoretical and experimental curves at $H = 0$ Oe was established. This is another distinctive feature of Bi-2223 ceramic superconductors that stands both for ''good'' samples of [2,12] and for our ''bad'' samples. It must be noted that, in spite of the fact that the theoretical returning curve in Fig. 10 does not seem to depart very much from the experimental one, it is only due to the scale employed.

5. Conclusions

A comparative study of the hysteresis of the transport critical current density in YBCO, Hg-1223 and Bi-2223 ceramics was performed. On one hand, the samples, whose microstructure was determined via scanning electron microscopy, show three different microstructural patterns, regarding grain shape, size and mutual disposition. On the other hand, the magnetic dependence of the critical current density shows a behavior that can be summarized in two different branches: YBCO and Hg-1223 have significant hysteresis, and the virgin, the saturated return and the flux trapping curves can be well described by the model explained in the text, employing a triangular shaped distribution of geometrical factors with predominance of the positives ones, while Bi-2223 shows weak hysteresis, and the model does not work so well. This behavior cannot be correlated with the micro structural findings. To our knowledge, this measurements are reported for the first time in the case of Hg-1223.

An interesting finding, not reported before in the literature, as far as we know, is the presence of an intergranular flux trapping ''tail'' in the low field part of the transport flux trapping curve for Hg-1223.

Acknowledgements

This work was partially supported by TWAS grant RG/PHYS/LA and by the University of Havana's ''Alma Mater'' program. M.T.D. Orlando acknowledges financial support from CNPq, FINEP, CAPES, CST, CVD and UFES.

References

[1] E. Altshuler, J. Musa, J. Barroso, A.R.R. Papa, V. Venegas, Cryogenics 33 (1993) 308.
[2] P. Muné, E. Altshuler, J. Musa, S. García, R. Riera, Physica C 226 (1994) 12.
[3] J. López, P. Muné, S. García, E. Altshuler, Physica C 272 (1996) 13.
[4] R.L. Peterson, W. Ekin, Phys. Rev. B 37 (1988) 9848.
[5] J.E. Evetts, B.A. Glowacki, Cryogenics 28 (1988) 641.
[6] K.H. Müller, D.N. Mathews, Physica C 206 (1993) 275.
[7] E. Altshuler, R. Cobas, A.J. Batista-Leyva, C. Noda, L. Flores, C. Martínez, M.T.D. Orlando, submitted to Phys. Rev. B.
[8] T. Henning, H. Kliem, A. Weyers, W. Bauhofer, Supercond. Sci. Technol. 10 (1997) 721.
[9] A. Sin, A.G. Cunha, A. Calleja, M.T.D. Orlando, F.G. Emmerich, E. Baggio-Saitovich, S. Piñol, J.M. Chimens, X. Obradors, Physica C 306 (1998) 34.
[10] A. Schilling, M. Cantoni, J.D. Guo, H.R. Ott, Nature 363 (1993) 56.
[11] M. Reder, J. Krelaus, L. Schmidt, K. Heinemann, H.C. Freyhardt, Physica C 306 (1998) 289.
[12] P. Muné, Ph.D. Thesis, University of Havana, Havana, 1996.
[13] J. Emmen, Ph.D. Thesis, Eindhoven University of Technology, Eindhoven, 1992.
[14] L.E. Flores, C. Martínez, Cryogenics 36 (1996) 705.
[15] P. Muné, E. Altshuler, J. Musa, Physica C 246 (1995) 55.
[16] E. Altshuler, S. García, J. Barroso, Physica C 177 (1991) 61.
[17] E. Altshuler, Ph.D. Thesis, University of Havana, Havana, 1994.
[18] Ch.P. Bean, Rev. Mod. Phys. 36 (1964) 31.
[19] E. Flores, E. Altshuler, S. García, J. Musa, Physica C 234 (1994) 368.
[20] A.J. Batista-Leyva, R. Cobas, M.T.D. Orlando, C. Noda, E. Altshuler, Physica C 314 (1999) 73.
[21] J.R. Clem, Physica C 153–155 (1988) 50.
[22] A.A. Zhukov, D.A. Komarkov, G. Karapetov, S.N. Gordeev, R.I. Antonov, Supercond. Sci. Technol. 5 (1992) 338.
[23] G.C. Kim, Y.C. Kim, Physica C 279 (1997) 122.
[24] Y.R. Sun, J.R. Thomson, H.R. Kerchner, D.K. Christen, M. Paranthaman, J. Brynestad, Phys. Rev. B 50 (1994) 3330.
[25] M. Reissner, Physica C 290 (1997) 173.
[26] P. Muné, J. López, Physica C 257 (1996) 360.
[27] P. Muné, J. López, E. Altshuler, Physica C 292 (1997) 48.
[28] E. Altshuler, S. García, A. Aguilar, Phys. Stat. Sol. (a) 120 (1990) K169.